







# Monitoring and Prediction of Coastal Rockfall Hazard: An Application of RocSlope3 in Newcastle (Australia)

Abigail Watman<sup>1</sup>, Davide Ettore Guccione<sup>1</sup>, Anna Giacomini<sup>1</sup> and Klaus Thoeni<sup>1</sup>

<sup>1</sup> Centre for Geotechnical Science and Engineering, The University of Newcastle, Callaghan, NSW 2308, Australia  
abigail.watman@uon.edu.au

**Abstract.** Rock mass instabilities – including rockfalls, wedge sliding failures and block topples – affecting sub-vertical rock cliffs in popular scenic coastal areas, significantly impact public safety and the financial viability of nearby assets. To effectively manage rockfall hazard along coastlines, it is essential to clearly understand the frequency and intensity of events impacting areas of interest. Because these rock slope instabilities are primarily controlled by the interaction of the coastal environment with pre-existing geostructural features, such as joints and bedding planes, detailed geostructural mapping and subsequent stability analyses provide indications of expected rockfall activity, complimenting existing rockfall monitoring techniques. This paper presents an application of RocSlope3 to a frequently visited coastal cliff in Newcastle, Australia, and directly compares the resulting expected rockfall activity to the observed events obtained via change detection analyses. Regular photogrammetric drone surveys yielded a series of high-resolution three-dimensional models of the site, facilitating extensive geostructural mapping of the cliff face and the identification of potentially unstable blocks. Characteristics of the predicted detachments from RocSlope3 – including volume and location – were compared with those of actual rockfall events identified via change detection analyses performed on the time series of rock slope models, further assessing the expected hazard.

**Keywords:** Rockfall, Change detection, Geostructural mapping, 3D kinematic analysis, Rocscience.

## 1 Introduction

Rock mass instabilities such as rockfalls, wedge sliding failures and block topples are highly hazardous events known to affect numerous sub-vertical rock cliffs in popular beaches and nature reserves along the Australian coastline. Such events pose significant risks to public safety and to the financial viability of nearby assets, including buildings and transportation infrastructure. A clear understanding of the frequency and intensity of rockfall events is fundamental to rockfall hazard assessment and mitigation endeavours along the coast. In recent years, rockfall inventories based on proximity remote sensing data (e.g. laser scanning and photogrammetry) have become the primary way

of deriving magnitude-frequency relationships [1], however, data of sufficient quality is not always available. Given that coastal rock slope instabilities are primarily driven by the interaction of the coastal environment with pre-existing geostructural features, such as joints and bedding planes, detailed geostructural mapping combined with three-dimensional kinematic analysis identifies potentially unstable blocks which may assist in the quantification of rockfall hazard in the absence of high-quality monitoring data [2]. To explore this possibility, this paper presents an application of RocSlope3 [3] to a frequently visited coastal cliff in Newcastle, Australia, and directly compares the resulting expected rockfall activity to the observed detachments obtained via photogrammetry-based change detection analysis.

## 2 Site Description

Nobbys Head is a prominent coastal headland, located near the harbour entrance and at the northern end of Nobbys Beach in Newcastle, NSW, Australia (**Fig. 1a**). The rounded cliff face is primarily composed of the characteristically blocky Nobbys Tuff unit overlain by the Victoria Tunnel Coal Seam, with a basaltic dyke striking north-west through the middle of the headland. The cliff is mostly unvegetated whilst the toe and adjacent beach are littered with blocks evidencing the history of frequent rockfalls. A small, non-protective wire mesh fence prevents pedestrian access to the cliff toe; however, this fence is frequently damaged or displaced by wave action. This case study considered an approximately 20 m high by 35 m long section on the south-eastern side of the headland (**Fig. 1b**).

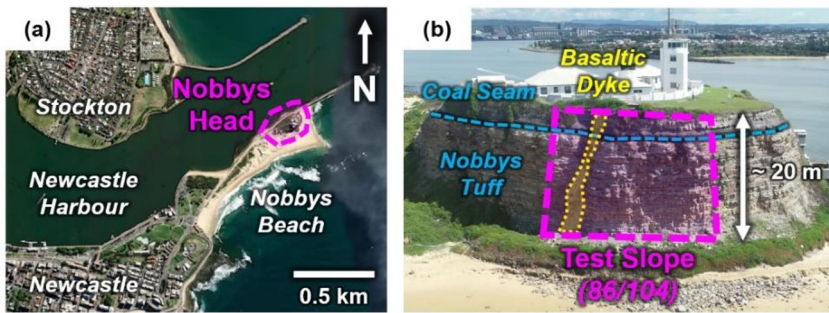


**Fig. 1.** (a) Site location within the Newcastle area (annotated aerial view from MinView). (b) Westerly view of Nobbys Head, showing key site features including the approximate test slope area with a dip and dip direction of 86/104 (degrees) in magenta, basaltic dyke in yellow and remaining site stratigraphy in blue.

### 3 Methodology

This case study relied on a time series of three-dimensional mesh models representing 26 approximately monthly photogrammetric drone surveys conducted between November 2022 and November 2024. For each survey, a series of high-resolution (20-mega-pixel) images were captured using a DJI Phantom 4 RTK drone via a series of automatic angled flights around 20 m away from the cliff slope. The three-dimensional mesh models were generated using Agisoft Metashape [4], involving the alignment (with GPS coordinates) and post-processing of the collected images. These mesh models were of high quality with a minimum mean vertex density of 1500 vertices/m<sup>2</sup>.

Detailed geostructural mapping was conducted using the earliest three-dimensional model (i.e. from November 2022) and Sirovision [5] to manually identify the centroid location, length and orientation of key discontinuities. Dips [6] enabled the identification and analysis of several joint sets and bedding planes.

Three-dimensional kinematic analyses, involving the identification of removable and potentially unstable blocks defined by the intersections of mapped discontinuities and the slope face, were subsequently performed in RocSlope3 [3]. For this purpose, 32 simulation scenarios (summarized in **Table 1**) were proposed to explore the influence of slope model type, type of mapped structures (named ‘raw discontinuities’ and ‘mean discontinuities’), and discontinuity radius (radius of circular disc around each discontinuity centroid). For ‘raw discontinuities’, each discontinuity had the mapped dip and dip direction, as opposed to ‘mean discontinuities’ where each discontinuity had a dip and dip direction corresponding to the mean orientation of its set (previously identified in Dips). Note that the mesh resolutions are high (mean density >1500 vertices/m<sup>2</sup>), low (mean density >600 vertices/m<sup>2</sup>) and simplified (10000 vertices total, achieved via the simplification tool in RocSlope3), whilst the simplified plane is a planar surface fit to the slope mesh. All bedding planes were assumed to be fully persistent, and their radius was set to 50 m to span the entire model width. All other discontinuity radii were either direct applications of the trace lengths obtained via mapping, or lengths modified to ensure minimum radii of  $R = 5$  m or  $R = 10$  m. In these latter cases, a radius equal to  $R$  was set for any discontinuities with mapped lengths below  $R$ .

External slope volumes were generated to ensure sufficient depth (>15 m) behind the slope surface for each simulation. Note that, a small depth behind the slope surface may not adequately capture the removable blocks. A typical friction angle of 30 degrees was adopted for kinematic analyses and all other RocSlope3 parameters were kept as default.

A custom Python script – employing the open3D [7] library – and a mask manually labelled in CloudCompare [8] were applied to automatically remove large vegetated areas, man-made structures and sand from each of the 27 three-dimensional mesh models. Change detection was performed on the 26 pairs of subsequent mesh models, using the recently developed VoxFall algorithm [9], available via a CloudCompare plug-in [8]. A voxel size of 0.05 m was selected. The slope azimuth was estimated via automatic plane-fitting in CloudCompare, yielding a slope dip direction of 104 degrees. False positive changes detected using VoxFall were manually removed by experienced practitioners, with reference to the mesh models and original aerial images.

**Table 1.** Summary of the simulations performed using RocSlope3.

| <b>Simulation</b> | <b>Slope type</b>    | <b>Mapping type</b>  | <b>Discontinuity radius, <math>R</math> [m]</b> |
|-------------------|----------------------|----------------------|---|
| S1                | High-resolution mesh | Raw discontinuities  | Mapped length                                   |
| S2                | High-resolution mesh | Raw discontinuities  | 2 x mapped length                               |
| S3                | High-resolution mesh | Raw discontinuities  | 5 m   |
| S4                | High-resolution mesh | Raw discontinuities  | 10 m  |
| S5                | High-resolution mesh | Mean discontinuities | Mapped length                                   |
| S6                | High-resolution mesh | Mean discontinuities | 2 x mapped length                               |
| S7                | High-resolution mesh | Mean discontinuities | 5 m   |
| S8                | High-resolution mesh | Mean discontinuities | 10 m  |
| S9                | Low-resolution mesh  | Raw discontinuities  | Mapped length                                   |
| S10               | Low-resolution mesh  | Raw discontinuities  | 2 x mapped length                               |
| S11               | Low-resolution mesh  | Raw discontinuities  | 5 m   |
| S12               | Low-resolution mesh  | Raw discontinuities  | 10 m  |
| S13               | Low-resolution mesh  | Mean discontinuities | Mapped length                                   |
| S14               | Low-resolution mesh  | Mean discontinuities | 2 x mapped length                               |
| S15               | Low-resolution mesh  | Mean discontinuities | 5 m   |
| S16               | Low-resolution mesh  | Mean discontinuities | 10 m  |
| S17               | Simplified mesh      | Raw discontinuities  | Mapped length                                   |
| S18               | Simplified mesh      | Raw discontinuities  | 2 x mapped length                               |
| S19               | Simplified mesh      | Raw discontinuities  | 5 m   |
| S20               | Simplified mesh      | Raw discontinuities  | 10 m  |
| S21               | Simplified mesh      | Mean discontinuities | Mapped length                                   |
| S22               | Simplified mesh      | Mean discontinuities | 2 x mapped length                               |
| S23               | Simplified mesh      | Mean discontinuities | 5 m   |
| S24               | Simplified mesh      | Mean discontinuities | 10 m  |
| S25               | Simplified plane     | Raw discontinuities  | Mapped length                                   |
| S26               | Simplified plane     | Raw discontinuities  | 2 x mapped length                               |
| S27               | Simplified plane     | Raw discontinuities  | 5 m   |
| S28               | Simplified plane     | Raw discontinuities  | 10 m  |
| S29               | Simplified plane     | Mean discontinuities | Mapped length                                   |
| S30               | Simplified plane     | Mean discontinuities | 2 x mapped length                               |
| S31               | Simplified plane     | Mean discontinuities | 5 m   |
| S32               | Simplified plane     | Mean discontinuities | 10 m  |

## 4 Results

Over 180 discontinuities were mapped within the slope area, revealing three near-vertical joint sets (89/069, 88/322, 88/019) and a set of near-horizontal bedding planes (1/190). The numbers of removable and unstable blocks identified via RocSlope3 modelling varied significantly across the 32 simulation scenarios (**Table 2**).

**Table 2.** Summary of block numbers and unstable block volume statistics determined via RocSlope3 modelling per simulation scenario. Simulations without valid blocks (S5, S13 and S29) are not reported.

| Simulation | Number of Blocks |           |          | Unstable Blocks Volume [m <sup>3</sup> ] |      |        |       |
|------------|------------------|-----------|----------|--|------|--------|-------|
|            | Valid            | Removable | Unstable | Min                                      | Max  | Median | Total |
| S1         | 8                | 4         | 0        | -  | -    | -      | -     |
| S2         | 29               | 11        | 0        | -  | -    | -      | -     |
| S3         | 1939             | 174       | 7        | 0.01                                     | 0.14 | 0.04   | 0.42  |
| S4         | 12419            | 174       | 18       | 0.01                                     | 0.04 | 0.02   | 0.32  |
| S6         | 3                | 3         | 0        | -  | -    | -      | -     |
| S7         | 1652             | 120       | 7        | 0.01                                     | 0.11 | 0.01   | 0.18  |
| S8         | 10212            | 492       | 7        | 0.01                                     | 0.05 | 0.02   | 0.17  |
| S9         | 8                | 4         | 0        | -  | -    | -      | -     |
| S10        | 41               | 16        | 4        | 0.01                                     | 0.03 | 0.02   | 0.08  |
| S11        | 2466             | 97        | 15       | 0.01                                     | 0.83 | 0.02   | 2.26  |
| S12        | 115              | 52        | 13       | 0.01                                     | 0.27 | 0.02   | 0.92  |
| S14        | 5                | 5         | 0        | -  | -    | -      | -     |
| S15        | 2023             | 164       | 8        | 0.01                                     | 0.3  | 0.045  | 0.75  |
| S16        | 11790            | 594       | 50       | 0.01                                     | 0.47 | 0.03   | 3.3   |
| S17        | 20               | 9         | 0        | -  | -    | -      | -     |
| S18        | 83               | 40        | 9        | 0.01                                     | 0.1  | 0.02   | 0.34  |
| S19        | 3257             | 460       | 212      | 0.01                                     | 0.83 | 0.02   | 9.84  |
| S20        | 15676            | 684       | 273      | 0.01                                     | 0.48 | 0.02   | 11.2  |
| S21        | 2                | 2         | 2        | 0.01                                     | 0.05 | 0.03   | 0.06  |
| S22        | 23               | 23        | 6        | 0.01                                     | 0.14 | 0.03   | 0.27  |
| S23        | 2732             | 680       | 210      | 0.01                                     | 0.38 | 0.03   | 10.21 |
| S24        | 1410             | 1410      | 432      | 0.01                                     | 0.47 | 0.02   | 18.03 |
| S25        | 21               | 9         | 0        | -  | -    | -      | -     |
| S26        | 60               | 19        | 0        | -  | -    | -      | -     |
| S27        | 619              | 148       | 9        | 0.01                                     | 0.1  | 0.03   | 0.32  |
| S28        | 8534             | 396       | 15       | 0.01                                     | 0.06 | 0.02   | 0.36  |
| S30        | 6                | 6         | 0        | -  | -    | -      | -     |
| S31        | 545              | 222       | 0        | -  | -    | -      | -     |
| S32        | 7261             | 586       | 0        | -  | -    | -      | -     |

As shown in **Table 2**, the simplified mesh simulations generated the most removable and unstable blocks, with the greatest total volumes, whilst the simplified plane was the least successful and tended to greatly underestimate the unstable block volumes. Within the same slope type and discontinuity radius, the raw and mean discontinuities appeared to generate similar results, with the latter often producing slightly more blocks and larger total volumes. Simulations with small discontinuity radii (i.e.  $R$  based on mapped

length) produced much lower numbers of removable and unstable blocks than those with large radii ( $R = 5$  m,  $R = 10$  m), with some simulations (S5, S13 and S29) not producing any valid blocks. It was noted, however, that in a thickly bedded rock unit such as Nobbys Tuff, large discontinuity radii could generate a series of elongated blocks between parallel joints from adjacent beds, and subsequent analyses of the unstable blocks would need to account for this.

269 detachments with volumes of  $0.005 - 6.8$  m<sup>3</sup> were detected via VoxFall. The observed detachment locations (VoxFall) and potentially unstable block locations of S24 (RocSlope3) are presented in **Fig. 2a** and **Fig. 2b**, respectively, whilst a comparison of the corresponding block volume distributions is depicted in **Fig. 3**. Note that the results for  $R = 5$  m are not depicted in **Fig. 3** as they are very similar to the results for  $R = 10$  m.

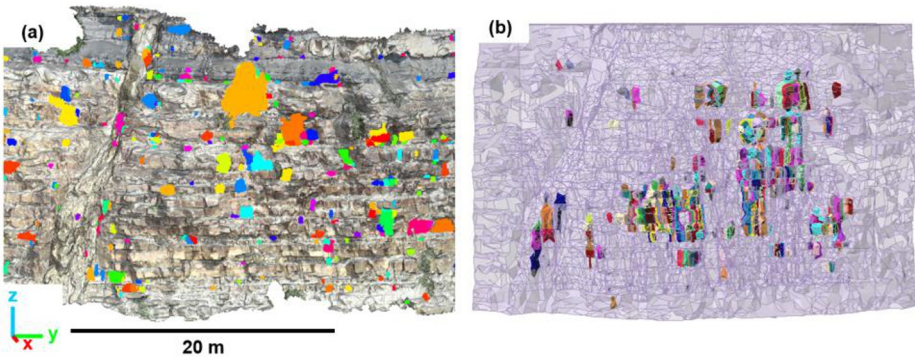


**Fig. 2.** Comparison of (a) detachments observed using VoxFall (colours represent the 26 distinct monthly monitoring periods) and (b) potentially unstable blocks identified for simulation S24 with RocSlope3 (random colours for distinct blocks).

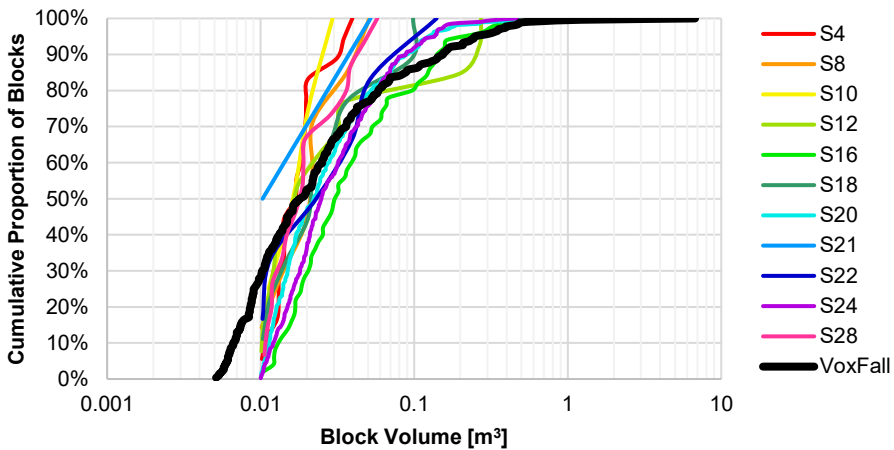


**Fig. 3.** Comparison of the proportions of unstable blocks up to certain volumes (cumulative block volume distributions) for several successful RocSlope3 simulations (excluding those with  $R = 5$  m) with the block volume distribution from VoxFall change detection analysis.

Considering the locations of observed detachments and potentially unstable blocks (**Fig. 2**), it seems that RocSlope3 predicted several of the observed detachment locations, however, many were not predicted. Whilst the RocSlope3 minimum volume explains the lack of predictions below  $0.01 \text{ m}^3$ , the remaining detachments appear not to be defined by visible discontinuities. Subsequent comparison of the cumulative block volume distributions for each RocSlope3 simulation (**Fig. 3**) revealed that simulations involving the simplified slope mesh and large discontinuity radii had volume distributions very similar to VoxFall. Overall, S20 and S24 appear to provide the most realistic distributions, with more potentially unstable blocks in S24 (mean discontinuities).

## 5 Conclusions

In this study, three-dimensional kinematic analyses were performed using RocSlope3 to explore their application in quantitative rockfall hazard assessment. The volume distributions of potentially unstable blocks were seen to be very similar to the distribution of detached volumes observed via a change detection analysis, particularly when a simplified mesh and large discontinuity radius (10 m) was used. With a good indication of the expected sizes of blocks defined by visible discontinuities and no sense of rockfall frequency, these analyses are not a direct substitute for detailed rockfall inventories but can instead complement a rockfall monitoring campaign or improve hazard estimates in cases where high-quality monitoring data is not available.

## Acknowledgements

This study was conducted with funding provided by the Australian Research Council (grant number DP210101122) and an Australian Government Research Training Program (RTP) Scholarship.

## References

1. Hantz, D., Corominas, J., Crosta, G. B., Jaboyedoff, M.: Definitions and Concepts for Quantitative Rockfall Hazard and Risk Analysis. *Geosciences*, 11(4), 158 (2021).
2. Lambert, C. Thoeni, K., Giacomini, A., Casagrande, D., Sloan, S.: Rockfall Hazard Analysis From Discrete Fracture Network Modelling with Finite Persistence Discontinuities. *Rock Mech Rock Eng*, 45, 871–884 (2012).
3. Rocscience. (2024). *RocSlope3 (1.006)*. [Software]
4. Agisoft. (2023). *Metashape (2.0)*. [Software]
5. Datamine. (2022). *Sirovision (6.2.2)*. [Software]
6. Rocscience. (2022). *Dips (8.019)*. [Software]
7. Zhou, Q., Park, J., Koltun V.: Open3D: A Modern Library for 3D Data Processing. arXiv:1801.09847 (2018).
8. Girardeau-Montaut, D. (2024). *CloudCompare (2.14.alpha)*. [Software]
9. Farmakis, I., Guccione, D. E., Thoeni, K., Giacomini, A.: A non-parametric change detection method for rockfall monitoring. In: 4<sup>th</sup> European Regional Conference of IAEG 2024.

**Open Access** This chapter is licensed under the terms of the Creative Commons Attribution-NonCommercial 4.0 International License (<http://creativecommons.org/licenses/by-nc/4.0/>), which permits any noncommercial use, sharing, adaptation, distribution and reproduction in any medium or format, as long as you give appropriate credit to the original author(s) and the source, provide a link to the Creative Commons license and indicate if changes were made.

The images or other third party material in this chapter are included in the chapter's Creative Commons license, unless indicated otherwise in a credit line to the material. If material is not included in the chapter's Creative Commons license and your intended use is not permitted by statutory regulation or exceeds the permitted use, you will need to obtain permission directly from the copyright holder.

